nature structural & molecular biology

Structural basis for heteromeric assembly and perinuclear organization of keratin filaments

Chang-Hun Lee[1,5], Min-Sung Kim[2], Byung Min Chung[1], Daniel J Leahy[2] & Pierre A Coulombe[1,3,4]

There is as yet no high-resolution data regarding the structure and organization of keratin intermediate filaments, which are obligate heteropolymers providing vital mechanical support in epithelia. We report the crystal structure of interacting 2B regions from the central coiled-coil domains of keratins 5 and 14 (K5 and K14), expressed in progenitor keratinocytes of epidermis. The interface of the K5–K14 coiled-coil heterodimer has asymmetric salt bridges, hydrogen bonds and hydrophobic contacts, and its surface exhibits a notable charge polarization. A *trans*-dimer homotypic disulfide bond involving Cys367 in K14's stutter region occurs in the crystal and in skin keratinocytes, where it is concentrated in a keratin filament cage enveloping the nucleus. We show that K14-Cys367 impacts nuclear shape in cultured keratinocytes and that mouse epidermal keratinocytes lacking K14 show aberrations in nuclear structure, highlighting a new function for keratin filaments.

Since their discovery, intermediate filaments have generated substantial interest owing to their diversity (>70 members) and differentiation-specific and context-related transcriptional regulation[1,2]. Such features, which are evolutionary conserved, have provided biologists and clinicians alike with a rich source of biomarkers to monitor differentiation in normal healthy tissues and in disease settings including cancer[3,4]. Interest in intermediate filaments was galvanized by the discovery of their direct involvement, upon mutation, in a broad range of diseases including many epithelial blistering disorders, cardiomyopathies, neuropathies and metabolic syndromes[2,4,5]. The phenotypes typifying these diseases reflect a loss or modulation of one or both of the two major functions fulfilled by intermediate filaments in the cytoplasm and nucleus: structural support, without which incident physical trauma exposes the inherent fragility and leads to loss of cell integrity, and regulation of several basic cellular processes (for example, cell growth, proliferation and apoptosis), made possible by interactions with various cellular proteins[6].

Although variable in size (40–240 kDa) and primary structure, all intermediate filament proteins feature a central α-helical rod domain of conserved length and substructure comprising four heptad repeat–containing segments (1A, 1B, 2A and 2B) interrupted by three short linker sequences (L1, L12 and L2) at conserved locations[7]. Although this central rod domain is the main driver that sustains self-assembly into filaments, the variable nonhelical domains located at the N-terminal (head) and C-terminal (tail) ends of intermediate filament proteins exert key roles in the assembly, organization and regulation of intermediate filaments, for example, via post-translational modifications and interactions with other proteins[8]. Intermediate filament proteins readily form coiled-coil dimers as they initiate polymerization, with the two participating chains aligned in parallel and in register[9,10]. Tetramer formation ensues as coiled-coil dimers interact along their lateral surfaces with an antiparallel orientation and staggered alignment, such that their coil 1B subdomains overlap[11,12]. The resulting structurally apolar tetramers are key assembly intermediates *in vitro* and *in vivo* (for example, refs. 12,13). Though the idealized model of intermediate filament structure consists of eight tetramers across partitioned into four distinct subfibrils, there is substantive evidence for structural polymorphism among intermediate filament polymers[14–16]. Intermediate filament proteins assemble into 10-nm filaments either as obligate or facultative heteropolymers *in vitro* and *in vivo*; many of them (for example, vimentin, desmin and nuclear lamins) can individually sustain the entire assembly pathway, yielding homopolymeric 10-nm filaments (for example, ref. 14).

Full-length intermediate filament proteins have not proven readily amenable to crystallization because of their polymerization-prone character, the absence of suitable inhibitors to trap intermediates and the structural polymorphism noted above. Such limitations prompted a 'divide-and-conquer' approach whereby discrete domains from intermediate filament proteins are selected for crystallization efforts[17]. This effort has met some success, and crystal structures are now available for the 2B subdomain of vimentin[10] and lamin A[18], the nonhelical tail domain of lamin A/C[19,20] and, more recently, the 1A subdomain and the partial coil 2 region of vimentin[21,22]. Notably, there is no structural information available yet for any heteropolymeric intermediate filament system, including keratins.

Type I (28 members) and type II (26 members) keratin proteins form 10-nm filaments as strict obligate heteropolymers, which calls for their coordinate expression in epithelial cells, where they

[1]Department of Biochemistry and Molecular Biology, Bloomberg School of Public Health, Johns Hopkins University, Baltimore, Maryland, USA. [2]Department of Biophysics and Biophysical Chemistry, Johns Hopkins University School of Medicine, Baltimore, Maryland, USA. [3]Department of Biological Chemistry, Johns Hopkins University School of Medicine, Baltimore, Maryland, USA. [4]Department of Dermatology, Johns Hopkins University School of Medicine, Baltimore, Maryland, USA. [5]Present address: College of Convergence, School of Basic Science, Daegu Gyeongbuk Institute of Science and Technology, Daegu, Korea. Correspondence should be addressed to P.A.C. (coulombe@jhsph.edu).

Received 18 November 2011; accepted 18 May 2012; published online 17 June 2012; doi:10.1038/nsmb.2330

are abundantly expressed and form intricate networks in the cytoplasm[4,23]. Most keratin genes are regulated in a pairwise-, tissue-type- and differentiation-dependent fashion in epithelia. One of the best understood keratin pairs is the type II K5 (58 kDa) and the type I K14 (50 kDa), expressed in the progenitor basal layer of stratified and pseudostratified epithelia[23,24]. K5 and K14 form extraordinarily stable dimer and tetramer subunits[25], and the resulting filaments can self-organize into cross-linked networks[26]. Dominantly acting missense mutations in either K5 or K14 cause epidermolysis bullosa simplex (EBS), the first intermediate filament–based genetic disorder to be identified[27]. In EBS, basal keratinocytes of epidermis and related epithelia rupture in response to frictional trauma, eliciting painful and debilitating blisters[28]. K5–K14 filaments are thus essential for maintenance of basal keratinocyte integrity in the face of mechanical trauma; this role has been found to apply to the entire intermediate filament protein superfamily. Here we report the crystal structure of a heterocomplex of the L2-2B domains from the K5 and K14 proteins. The resulting model not only provides insight into the heteromeric character of K5–K14 coiled-coil dimers but also reveals the occurrence of a *trans*-dimer disulfide bond bridging K14 molecules that is poised to contribute to the organization of keratin filaments in the perinuclear cytoplasm, with an associated impact on the size and shape of the nucleus.

RESULTS

Unique features of K5–K14 2B heterodimeric coiled coil

We crystallized a complex of K5 L2-2B and K14 L2-2B (**Fig. 1a**), which behaves as a functional assembly intermediate *in vitro* and *in vivo* (**Supplementary Fig. 1a–c**). The resulting structure includes residues Thr382–Gly476 of K5 and Ser332–Gly421 of K14 (**Supplementary Fig. 1d**). The L2 region and N-terminal end of the 2B domains of K5 and K14 are not well ordered in the crystal, and we did not model them. X-ray data collection and refinement statistics are reported in **Table 1**. The structure of the 2B domain of K5–K14 reveals a typical left-handed coiled-coil dimer, with the two α-helices oriented in parallel and in register (**Fig. 1b**) and one coiled-coil heterodimer of K5–K14 2B domains per asymmetric unit.

Examination of the interface between the K5 and K14 chains revealed the unique character of the K5–K14 2B coiled coil. Consistent with established principles of coiled-coil architecture[29–31], extensive apolar interactions occur between residues located in the A and D positions of heptad repeats (ABCDEFG) in the intertwined 2B helices (**Fig. 1c**). In addition, electrostatic interactions and hydrogen bonds occurred between K5 and K14 in that interface (**Fig. 1c** and **Supplementary Table 1**). Salt bridges between G and E′ are common in coiled-coil structure[29–31], but hydrogen bonds and water-mediated interactions between the participating monomers are not anticipated. The C terminus of the molecule displayed extensive interactions via intrachain and interchain salt bridges. This evolutionarily conserved region is believed to act a 'trigger motif', nucleating coiled-coil assembly of the participating 2B coils from intermediate filament proteins[32].

The K5–K14 2B heterocomplex forms more readily, and is markedly more stable in solution, relative to K5 or K14 2B homodimers (data not shown; ref. 25). Homology modeling using the K5–K14 crystal structure as a template revealed that three of the five salt bridges and hydrogen bonds occurring between K5 and K14 monomeric helices would be lost in the K5 and the K14 homodimers (**Supplementary Fig. 2a**). Salt bridges would be maintained in the C-terminal trigger motif[32]. Electrostatic interactions involving residues located in the trigger motif are likely essential for initiating dimerization and setting the axial alignment of the two participating α-helices, as proposed[32], whereas a distinct set of electrostatic interactions occurring along two monomer chains is poised to stabilize the K5–K14 heterodimer (see below).

The hydrogen bonds and most of the salt bridges in the K5–K14 model are unidirectional or asymmetric, which sets the keratin 2B heterodimeric coiled coil apart from the vimentin and other homodimeric coiled coils (**Fig. 1c** and **Supplementary Fig. 2a**,**b**). Only symmetric salt bridges occur at the interface of the vimentin 2B coiled coils. The K5–K14 heterodimer features more salt bridges, all of which are asymmetric, along with fewer symmetric hydrophobic interaction clusters ('islands'; **Supplementary Fig. 2b** and

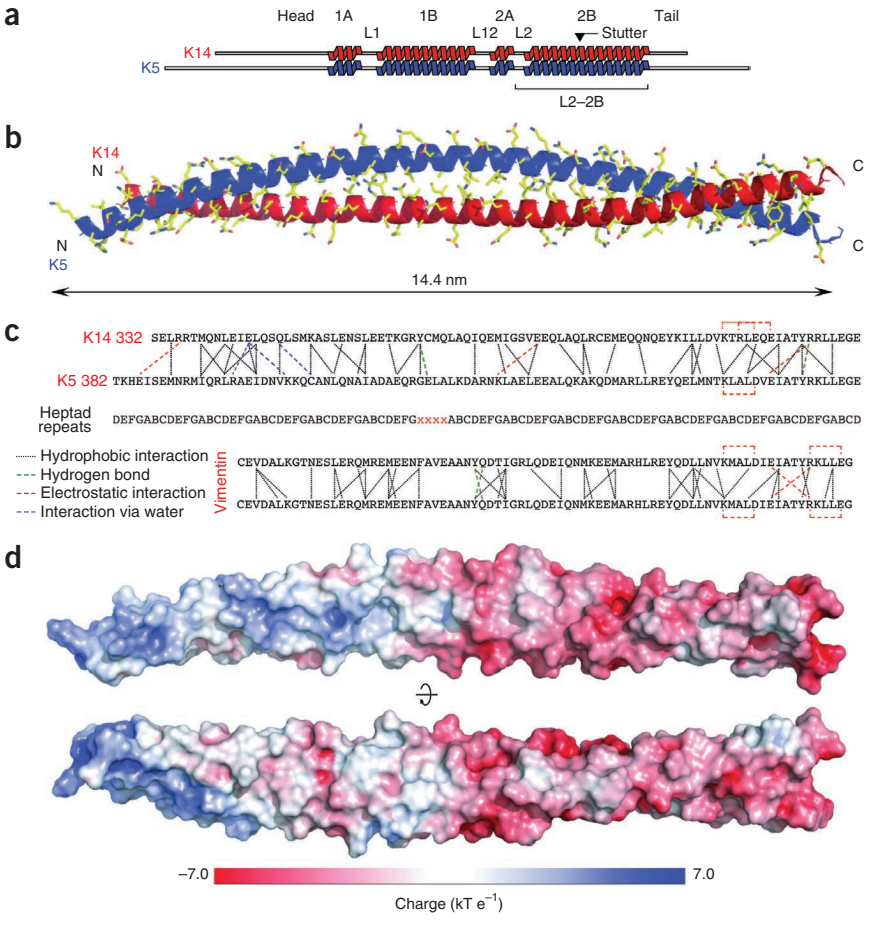

Figure 1 K5 and K14 domain structure, and crystal structure of the K5–K14 2B heterocomplex. (**a**) Schematic diagram of the domain structure of K5 and K14. (**b**) Crystal structure of the K5–K14 coil 2B heterocomplex. (**c**) Interactions occurring at the interface of the K5–K14 heterodimer (top; this study) and vimentin homodimer (bottom; PDB 1GK4 from ref. 10). (**d**) Electrostatic surface potential of the K5–K14 coil 2B complex.

Table 1 Data collection, phasing and refinement statistics

	Native	SeMet
Data collection		
Space group	*H*32	*H*32
Cell dimensions		
a,*b*,*c* (Å)	150.99, 150.99, 141.62	150.60, 150.60, 141.75
α,β,γ (°)	90, 90, 120	90, 90, 120
		Peak (SAD)
Wavelength	0.97944	0.97944
Resolution (Å)	3.0 (3.11–3.00)[a]	3.0 (3.11–3.00)
R_{sym}	8.5 (67.9)	5.9 (32.3)
$I / \sigma I$	15.55 (1.47)	28.2 (2.02)
Completeness (%)	98.8 (91.1)	89.9 (42.4)
Redundancy	7.0	8.2
Refinement		
Resolution (Å)	30–3.0	
No. reflections	12,538	
R_{work} / R_{free}	20.91/23.35	
No. atoms		
Protein	1,504	
Water	6	
B-factors		
Protein	114.0	
Water	83.4	
R.m.s. deviations		
Bond lengths (Å)	0.006	
Bond angles (°)	0.8	
Ramachandran analysis		
Most favored (%)	174 (97.8%)	
Allowed (%)	4 (2.2%)	
Generously allowed (%)	0	
Disallowed (%)	0	

[a]Highest resolution shell is shown in parentheses.

Supplementary Note). These unique features likely act as a strong positive force that favors heterodimerization of K5 and K14 α-helices. The importance of several of the electrostatic interactions revealed in our crystal structure is supported by previous biochemical studies of K5 and K14 point mutants[32,33] (**Supplementary Fig. 2c**).

Mapping of surface charges in the K5–K14 2B coiled coil revealed a notable polarization. Calculated pI values suggest that the 2B domains of K5 and K14 should bear an overall high negative charge (5.80 and 4.69, respectively). In the crystal structure, however, the K5–K14 2B coiled coil shows a strong negative charge potential at the C terminus and a strong positive charge potential at the N terminus (**Fig. 1d**). Both K5 and K14 contribute to the polarized surface potential of the 2B coiled coil, in a complementary fashion. This dramatic bias in surface-charge distribution does not occur in the crystallized 2B domains of lamin A/C[18] or vimentin[10] and likely influences the axial alignment of K5–K14 dimers as they interact to form larger oligomers.

Implications for epidermolysis bullosa simplex

Mapping the location of EBS-causing amino acid substitutions in the K5–K14 2B crystal structure enabled a correlation of keratin structure and function and a deeper level of insight into the underlying pathogenesis. We carried out this analysis for several EBS-causing missense mutations mapping to the 2B region of K5 and K14 (http://www.interfil.org/ and ref. 5), relating them to the severity (that is, clinical subtype) of EBS they generate: EBS-localized (mild), EBS-generalized (intermediate severity) and EBS-DM (the most severe and occasionally lethal Dowling-Meara form) (**Fig. 2a** and **Supplementary Table 2**). The vast majority of EBS cases are caused by dominantly acting missense alleles, irrespective of disease severity[28]. Relevant EBS-related mutations in the coil 2B of K5 and K14 clearly partition to one of two regions, the middle portion (near the stutter) and the C-terminal end (**Fig. 2b**), and can be segregated into two major types, interface mutants and surface-exposed mutants. Moreover, the K5–K14 2B crystal structure revealed that many of the EBS disease-causing mutations impact residues whose side chains directly interact within the coiled-coil interface (**Fig. 2c**,**d**).

Interface mutants typically have mutated amino acids whose side chains are engaged in either a hydrophobic, electrostatic or hydrogen-bond contact (**Supplementary Table 2**). This group of mutants includes two salt-bridge mutants, K5-E466D (EBS-generalized) and K14-R416P (EBS-DM), which is associated with severe EBS, underscoring the crucial importance of this contact. The more severe impact of K14-R416P might reflect the combined effect of helix breaking and the loss of a salt bridge. Otherwise, we note that 'conservative' substitutions to a different hydrophobic group (for example, in K5-I467M (EBS-generalized), K5-I467L (EBS-localized) and K14-L408M (EBS-localized)) can engender varying degree of disease severity, conveying that in such cases specific hydrophobic contacts or steric hindrance are crucially important. For example, mutations in K5-I467M and K14-L408M may generate an impact owing to the length difference originating from an additional methyl group plus sulfur. Such substitutions, although conservative, may cause a substantial clash with other chemical groups in a highly packed context with limited freedom with regard to side chain flexibility. K5 Ile467 is close to Leu408 of K14 (3.5 Å apart, no hydrogen atom), and it is buried by Glu401 of K14. Elongation of the side chain in this position may thus generate a clash with Leu408 or Glu401 of K14 and require remodeling of this interface. Likewise, K14 Leu408 is close to Ile467 of K5 and Val404 of K14, and it is surrounded by Lys460 and Asp464 of K5 (distances 3.6–3.9 Å). Even a modest lengthening of the side chain at positions such as K5 Ile467 and K14 Leu408 may trigger a remodeling of the local coiled-coil interface, which, when cumulated in space as several dimers further interact during assembly of 10-nm filaments, alters the structure and/or properties of the final polymer. Mutations affecting residues with surface-exposed side chains (**Supplementary Table 2**) are expected to have no impact on dimer structure and instead affect the formation and/or structure on higher-order oligomers.

At the C terminus of the 2B domain lies a defining sequence motif, TYRKLLEGE, that is near-perfectly conserved among all intermediate filament proteins (**Supplementary Fig. 1d**), is important in 10-nm filament assembly[34] and is frequently targeted by mutations in intermediate filament–based diseases (**Fig. 2a**, **Supplementary Table 2** and ref. 5). This region features a dense array of non-hydrophobic interactions between the K5 and K14 strands, considerably denser than the corresponding region in the vimentin and lamin A/C crystals (**Supplementary Fig. 2**). The spectrum of EBS-causing mutations reveals that there is low tolerance for side chain modifications in this motif and also that small alterations in side chain chemistry may trigger large differences in EBS severity (**Fig. 2a** and **Supplementary Table 2**). Many mutations occurring in K5's TYRKLLEGE motif affect surface-exposed residues (for example, T569P, R471C, E475K, E475G and G476D; **Supplementary Table 2**). This region in K5 may therefore be an important biochemical anchor for interacting coiled-coil dimers during filament assembly.

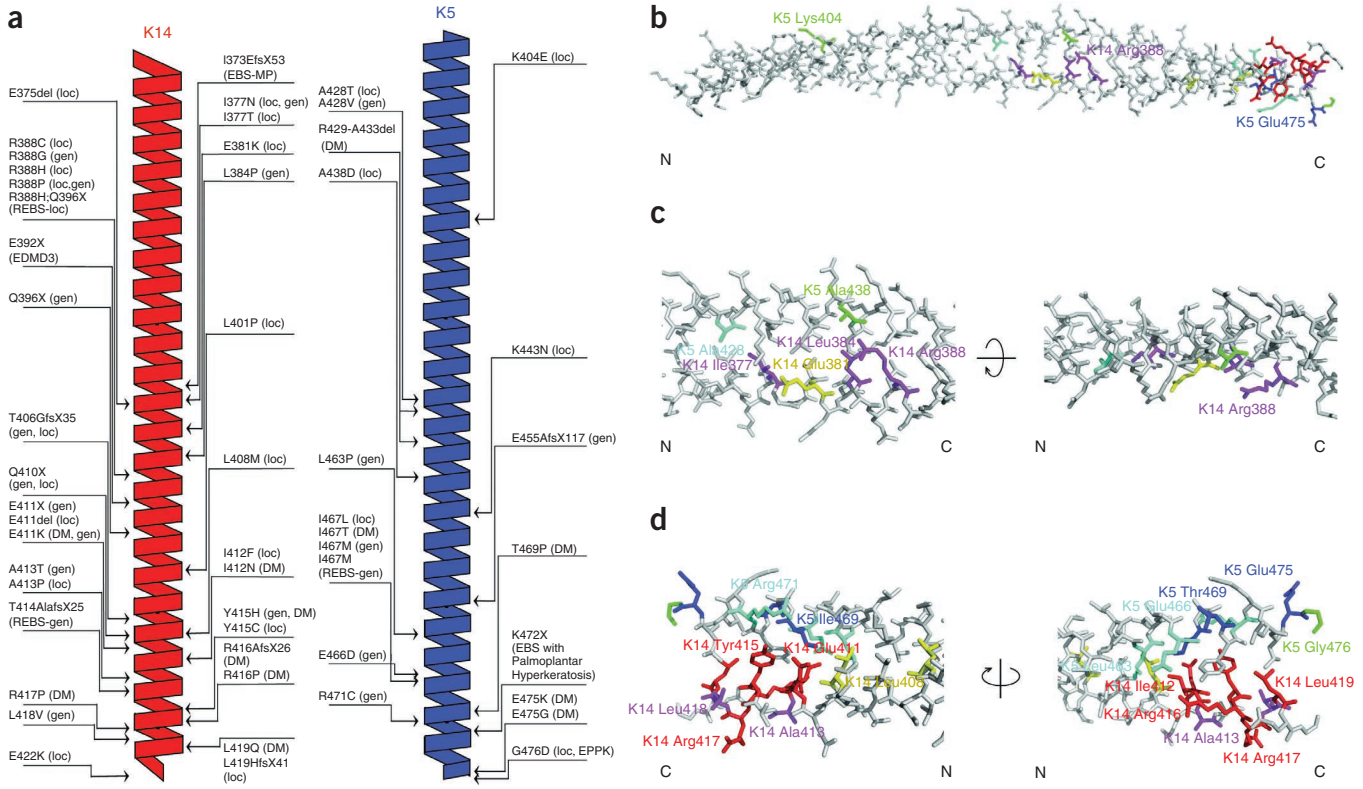

Figure 2 Structure-function relationship of EBS. (**a**) EBS-causing mutations mapped to the 2B coils in K5 and K14. (**b**) Mapping of a subset of mutations to the structural model of K5–K14 2B coiled coil. Types of mutations, based the severity of the effects, were designated as follows: pale color for severe EBS-general (gen); original, dark color for EBS-DM; bright color for mild EBS-local (loc); cyan, blue and green for K5; and magenta, red and yellow for K14. (**c**) Mapping of a cluster of interesting mutations near the stutter. (**d**) Mapping of cluster of mutations near the C-terminal end, which feature the highly conserved LLEGE motif.

Occurrence of a homotypic disulfide bond via K14 Cys367

Two symmetry-related K5–K14 heterodimeric coiled coils were conjugated to each other in the crystal, giving rise to an 'X'-shaped structure (**Fig. 3a**). The electron density map showed that the two keratin coiled coils were linked via a single homotypic disulfide bond involving Cys367 in K14 (**Supplementary Fig. 3a**). Nonreducing SDS-PAGE analysis confirmed the presence of an additional, larger species corresponding to the predicted size of a dimer in the crystal (**Fig. 3b**). This dimer-sized band reverted to monomers in the presence of the reducing agent Tris-(2-carboxyethyl)phosphine (TCEP). Only the K14 L2-2B-tail protein, not K5 L2-2B, contributed to the dimer-sized species under oxidative conditions (**Fig. 3b**). The lone cysteine residue in K5's 2B domain (Cys407) has its side chain buried at the dimer interface. Of the two cysteines located in K14's 2B domain, Cys367 and Cys389, only the former forms a disulfide bond in the crystal (**Supplementary Fig. 3b**). K14 Cys367 is located in the stutter region, a four-residue interruption of the heptad repeat conserved in the 2B domain of all intermediate filament proteins. The occurrence of a cysteine residue at this position in human K14 is conserved in its mammalian orthologs and in epidermal type I keratins, including K10 (**Fig. 3c**). These findings are intriguing given that the stutter, which has no obvious impact on the helical pitch in intermediate filament protein coiled coils (our results and refs. 10,18), is believed to allow for increased local dynamic flexibility in the coiled-coil fold[35].

Disulfide-bonded, native keratin species have been evidenced more than 30 years ago in serially cultured human skin keratinocytes[36]. We report here that this also occurs in mouse skin keratinocytes. The two major epidermal type I keratins, K14 and K10, occurred as disulfide-bonded dimers in mouse epidermis *in situ* (**Fig. 3d**). In keratinocytes freshly isolated from newborn mouse epidermis, disulfide-bonded K14 preferentially partitioned to the insoluble (polymerized) pool of keratin proteins (**Supplementary Fig. 3c).** Cell-transfection assays designed to assess *de novo* 10-nm filament formation in fibroblasts (which are keratin-negative) and incorporation into pre-existing filaments in skin keratinocytes conveyed that K14-C367A and K14-C389A variants were assembly-competent (**Supplementary Fig. 3d**). In lysates prepared from transfected mouse keratinocytes and analyzed by nonreducing SDS-PAGE, GFP–K14-C367A was associated with a markedly lower yield of disulfide-bonded K14 homodimers, relative to wild-type K14 and K14-C389A (**Fig. 3e**). We conclude that Cys367 has a key role in the formation of a specific, disulfide-bonded K14 homodimeric species in living cells.

Disulfide-linked K14 homodimers occurred at a low stoichiometry (~5% of total K14 levels) in mouse skin keratinocytes at baseline (**Fig. 3d**,**e**). Their levels were markedly increased by elevating calcium concentration in the culture medium (**Fig. 4a**), a condition that promotes cell-cell adhesion within minutes and terminal differentiation within 1–2 d (ref. 37), but were unresponsive to various forms of cellular stress including osmotic shock and oxidative stimulus (data not shown). The observation that at least 8 h of exposure to higher calcium concentration was necessary to increase the levels of disulfide-linked K14 homodimers (**Fig. 4a**) suggests that the physiological importance of this species in skin keratinocytes is related to terminal differentiation, rather than cell-cell adhesion.

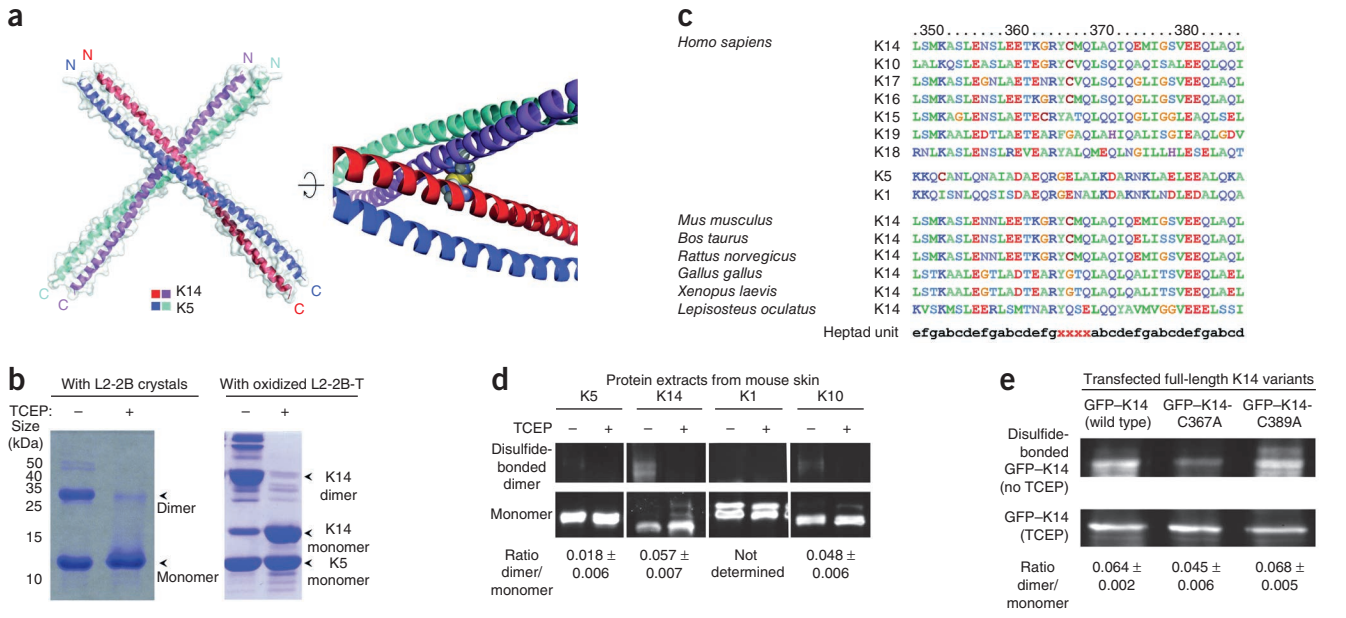

Figure 3 A *trans*-dimer, K14 Cys367–mediated homotypic disulfide bond in the K5–K14 structure. (**a**) A coiled-coil dimer and its symmetry related pair occur in the crystal. The disulfide bond via K14 Cys367 is highlighted with a space-filling model on the right. (**b**) Nonreducing SDS-PAGE analysis of pooled crystals of the K5–K14 heterocomplex (left) and of the phenanthroline-oxidized K5–K14 L2-2B-tail (T) (right). (**c**) Sequence alignment of type I keratins and selected type II keratins expressed in epidermis. K14 sequences from various species are aligned as well, relative to the heptad units. (**d**) Nonreducing SDS-PAGE coupled with western blotting of proteins from mouse skin *in vivo*. (**e**) Analysis similar to **d**, except that the proteins were obtained from mouse 308 keratinocytes transiently transfected with wild-type K14, K14-C367A and K14-C389A fused to GFP. The unconjugated monomer band (TCEP blot) was visualized by using diluted samples (1:10) of the original protein solution to avoid oversaturated signal. For **d** and **e**, ratios of protein dimer band over monomer band were determined by densitometry; shown is the average ± s.d. from three (**d**) or four (**e**) independent experiments.

A disulfide-linked keratin filament cage around the nucleus

We adapted a differential labeling method to localize disulfide bonds in the cytoskeletal (insoluble) compartment of mouse skin keratinocytes in culture. Specific staining for disulfide-bonded 'insoluble' proteins occurred primarily as puncta throughout the cytoplasm and nucleus of keratinocytes (**Fig. 4b**), reflecting in part their known prevalence in the endoplasmic reticulum[38]. Co-localization of disulfide bonds with K14-positive filaments was markedly enhanced in high-calcium medium and was concentrated around the nucleus (**Fig. 4b**). The prominent K14-positive filament bundles occurring elsewhere in the cell, particularly under low-calcium culture conditions, only infrequently co-localized with disulfide bonds (**Fig. 4b**). Next we solubilized proteins from keratinocyte cultures processed for the *in situ* labeling of disulfide-bonded proteins with Alexa Fluor 594, and we immunoprecipitated the resulting lysates for K14 antigens. As expected, a greater amount of Alexa Fluor 594–derivatized K14 protein occurred in immunoprecipitates from keratinocytes cultured under high-calcium medium conditions (**Fig. 4c**; 1.42 ± 0.03–fold increase; average ± s.d.; $n = 3$ replicates). Analysis of nuclei isolated from mouse keratinocytes confirmed the perinuclear enrichment of disulfide-linked K14 dimers (**Fig. 4d**). These findings together establish that disulfide-bonded K14 species are concentrated in the perinuclear network of keratin filaments in skin keratinocytes in culture.

In skin keratinocytes, key attributes are modulated in a consistent fashion depending on culture conditions. In low-calcium medium, keratinocytes have thick and straight bundles of keratin filaments that run parallel to the main axis of the cell and are more likely to contain an ellipsoid-shaped nucleus (**Supplementary Fig. 4a** and **Supplementary Movie 1**). In high-calcium medium, by comparison, keratin-filament bundles tend to wrap tightly around round-shaped nuclei, where they cross one another at various angles to form a cage-like structure (**Supplementary Fig. 4b**,**c** and **Supplementary Movie 2**). Several factors suggest that the K14 Cys367–mediated disulfide bond forms between, rather than within, filaments organized in a specific configuration at or near the nuclear surface (see below).

We next analyzed epidermis of a newborn mouse using the differential staining method for disulfide bonds. We observed a positive signal for such bonds in keratinocytes throughout the epidermis, with a higher staining intensity clearly and consistently occurring in the lowermost suprabasal layers (**Fig. 5a**). This region of the epidermis, and in particular the very first suprabasal layer, also featured the most compelling colocalization of the signals for cystine bonds and K14 antigens (**Fig. 5a**). In epidermis of a wild-type newborn mouse, the cross-sectional area of the nucleus steadily increased as keratinocytes moved from the basal to first suprabasal layer and then to the remaining (upper) suprabasal layers (**Fig. 5b**). Aspect ratio measurements showed that keratinocyte nuclei adopted a rounder shape selectively in the first suprabasal layer of the epidermis (**Fig. 5c**). This phenomenon was transient, as nuclei regained a more ellipsoid shape in the upper suprabasal layers (**Fig. 5c**). These findings emulate those obtained as a function of calcium concentration in cultured mouse skin keratinocytes (**Supplementary Fig. 4**).

We repeated these analyses in tissue sections prepared from the skin of newborn K14-null pups and their control littermates, to assess whether the loss of K14 impacts any of these cytoarchitectural attributes. We made several compelling observations. First, the staining intensity for cystine was markedly reduced in the basal layer of K14-null epidermis (mean pixel intensity in K14-null epidermis sample was 8.06 ± 4.10 and in wild type, 17.51 ± 4.92), implying that a large fraction

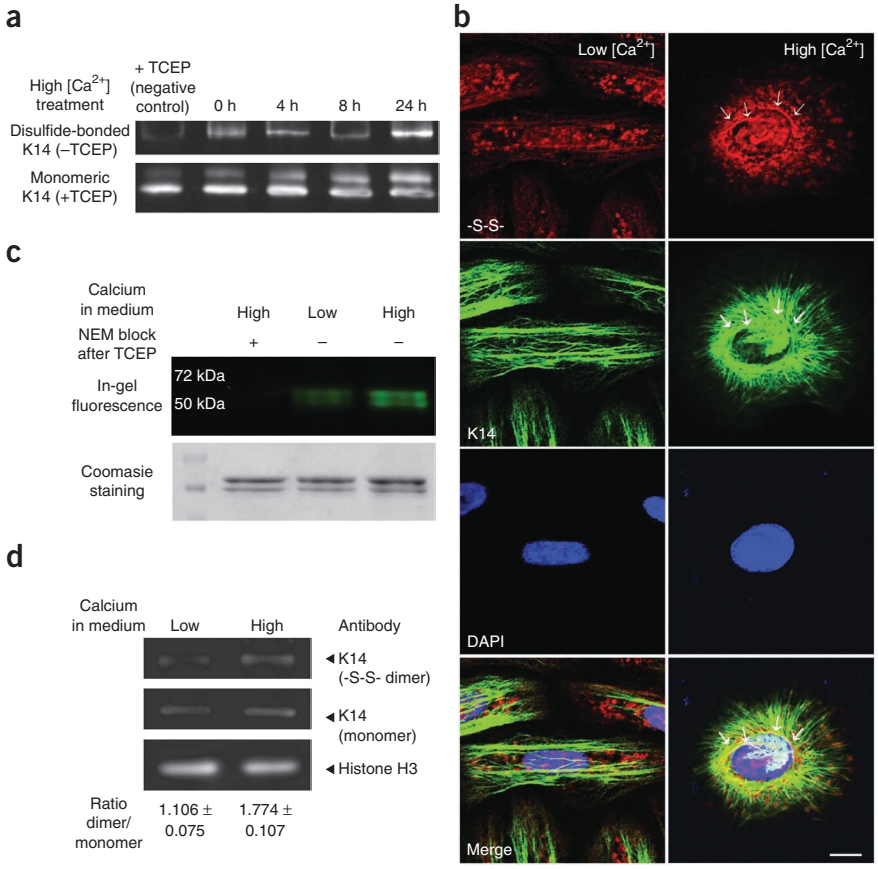

Figure 4 Calcium-dependent regulation and localization of the keratin-associated disulfide bond. (**a**) Western blot to analyze the impact of calcium treatment, for indicated amounts of time, on the yield of homotypic K14 disulfide bond in mouse 308 keratinocytes in culture. (**b**) Fluorescence microscopy analysis to locate disulfide-bonded keratin in mouse 308 keratinocytes in culture; free sulfhydryl group–specific dye, Alexa Fluor 594 C_5-maleimide, was used to label chemically exposed disulfide-bonded (-S-S-) cysteine residue(s) in medium with indicated calcium conditions. Arrows indicate co-localization of cystine and K14 signals. Scale bar, 10 µm. (**c**) SDS-PAGE analysis of K14, immunoprecipated using a K14-specific antibody, from cells cultured in either low- or high-calcium-concentration medium and processed for Alexa Fluor 594 C_5-maleimide–mediated staining of disulfide bond, as described in **b**. After in-gel fluorescence assay, the gel was stained with Coomassie blue dye to convey protein loadings. NEM, *N*-ethylmaleimide. (**d**) Western blot of nuclear proteins prepared from mouse keratinocytes. Nuclei were isolated from keratinocytes cultured in low- or high-calcium-concentration medium using sucrose density gradient centrifugation and buffer conditions that favor keratin disassembly (pH 9.0). Nuclear protein extracts were subjected to nonreducing SDS-PAGE and western blot. Histone H3 was used as loading control. Ratios of K14 dimer band over monomer band were determined by densitometry (average ± s.d. from three independent experiments).

of the disulfide bonds present in basal keratinocytes occurred in a K14-dependent fashion (**Fig. 5a**). No substantial difference in disulfide-bond staining occurred for the suprabasal layers (**Fig. 5a**), a finding that may reflect the presence of normal levels of K10. Second, the nucleus was significantly smaller in keratinocytes located in the basal ($P < 0.0001$) and first suprabasal ($P < 0.02$) layers of newborn-mouse K14-null epidermis, relative to wild-type epidermis (**Fig. 5b**). Third, there was a significant decrease ($P < 0.0001$) in the extent to which the nucleus rounded up in keratinocytes from the first suprabasal layer of K14-null epidermis (**Fig. 5c**). These findings show that loss of K14 is associated with layer-specific alterations in the density of disulfide bonds, and in the size and shape of keratinocyte nuclei in K14 null epidermis *in vivo*.

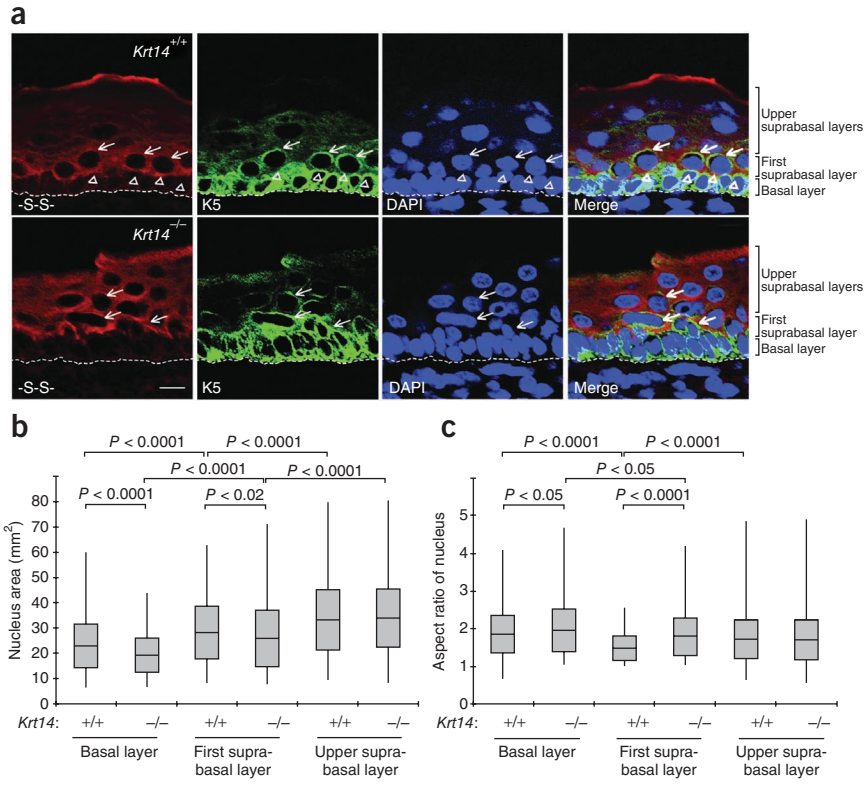

Figure 5 Localization of the keratin-associated disulfide bond in newborn-mouse epidermis, and impact of K14 loss on nuclear size and shape. (**a**) Micrographs of skin sections prepared from postnatal day 2 (P2) mouse littermates, wild type (*Krt14*$^{+/+}$) and null (*Krt14*$^{-/-}$), with Alexa Fluor 594 C_5-maleimide–mediated staining of disulfide bond (-S-S-; see **Fig. 4**). Scale bar, 10 µm. Dotted line marks the dermo-epidermal interface. Arrowheads, nuclei in basal layer; arrows, nuclei in suprabasal layer. (**b**,**c**) Measurement of the surface area (**b**) and aspect ratio (an indicator of shape; **c**) of keratinocyte nuclei in the epidermis of P2 *Krt14*$^{+/+}$ and *Krt14*$^{-/-}$ P2 mouse littermates from **a**. Data are reported as box-and-whisker plots with means, ± s.d., maxima and minima. The values are from 300 nuclei sampled from two littermates and four different sections from scalp skin per each genotype.

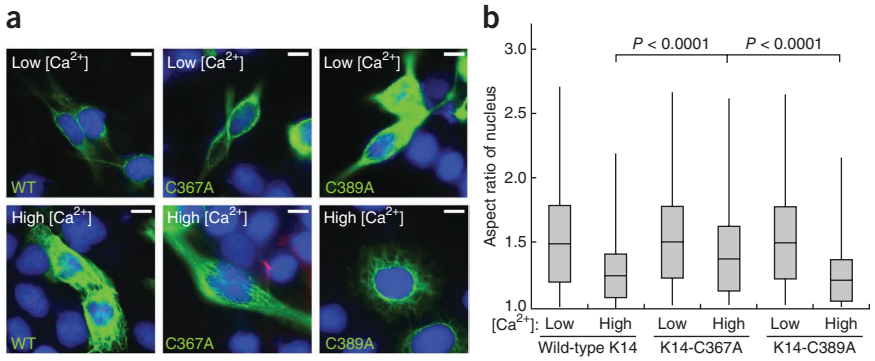

Figure 6 Direct linkage of K14 Cys367 and the maintenance of the round nuclear shape under high calcium medium. (**a**) Immunofluorescence micrographs of A431 human keratinocytes depleted for its major type I keratin, K17 (by *Ker17* shRNA; Online Methods), reconstituted with either wild-type GFP-K14 (WT) or one of two GFP-fused K14 variants (C367A or C389A) and cultured in low- or high-calcium-concentration medium. Stainings are as follows: green, K14 variants; blue, DAPI (nuclei); red, K17. Scale bars, 10 μm. (**b**) Assessment of nuclear shape by determination of the aspect ratio. Data are reported as box-and-whisker plots with means, ± s.d., maxima and minima. At least 300 nuclei from K17-negative, GFP (K14)-positive cells were analyzed for each condition tested.

Finally, we devised an assay to test whether K14 Cys367 has a role in the determination of nuclear shape in keratinocytes. For this, we produced an A431 keratinocyte cell line variant with stable short-hairpin (sh)RNA-mediated knockdown of mRNA that encodes K17 (ref. 39) (this cell line otherwise expresses the type I K18, which does not feature a cysteine residue in its 2B stutter motif, and expresses K14 at very low levels[24]; **Fig. 3c**). Transfection-mediated expression of wild-type K14 in these cells results in its recruitment into filaments (**Fig. 6a**) and, upon switching to high-calcium medium, to a rounding of the nuclear shape, as assessed from the aspect ratio (**Fig. 6b**). Relative to wild-type K14–expressing and K14-C389A–expressing A431 cells with knockdown of the mRNA that encodes K17, cells expressing K14-C367A maintained a more ovoid nuclear shape upon switching to high-calcium medium, a significant ($P < 0.0001$) finding (**Fig. 6**). These findings formally connect Cys367 of K14 to the shape of the nucleus in calcium-responsive keratinocytes.

DISCUSSION

All intermediate filament proteins are typified by a high α-helical content along with long-range heptad repeats in their centrally located rod domain, which is conserved in length and substructure. In 1952, Francis Crick suggested the coiled-coil mode of interaction between alpha helices based on the X-ray diffraction pattern of hair keratin[40]. Virtually all of his pioneering insight has been confirmed 40 years later, when the atomic structure of the GCN4 coiled coil became available[41]. Why some intermediate filament proteins form homodimeric coiled coils whereas many others heterodimerize, in either a strict or facultative fashion, as they initiate assembly into 10-nm filaments, is unknown from both structural and functional perspectives. The availability of atomic-level insight into the structure of the 2B coiled coil for lamin A[18], vimentin[10] and a keratin pairing (K5–K14; this study) provides an opportunity to speculate on the biochemical determinants supporting the heteromeric versus homomeric pathway of dimer formation (**Supplementary Fig. 2**).

The 'X'-shaped architecture of interacting dimers in the keratin crystal and the finding of a specific *trans*-dimer, K14-mediated disulfide bond at the point of contact between coiled-coil dimers are the major unanticipated findings of this study. The residue involved, K14 Cys367, is located in the stutter, a four-residue segment that disrupts the heptad repeat at a conserved location in the 2B domain of all intermediate filament proteins. A discontinuity of the heptad (or undecad) repeat, termed a stutter or stammer, occurs in many atomic models of proteins with coiled-coil motifs[30]. Although stutters usually do not disrupt the α-helical structure of coiled coils, molecular dynamics studies suggest that they locally enhance flexibility, allowing for local 'breathing' or increased motion of the coiled coil[35]. The only function so far ascribed to the conserved stutter present in intermediate filament proteins is to maintain a proper register of the helix surface, for instance, loss of the stutter (by the addition of three amino acids) compromises the filament-forming potential of vimentin, in spite of the maintenance of helical structure[42]. As K14 Cys367 is conserved in many other type I keratins expressed in epidermis and related stratified epithelia, it is likely that the findings reported here have broad implications for the biology of keratins. The occurrence of residual disulfide bonds involving K14 Cys367 (**Fig. 3e**) suggests that additional cysteine residues in K5 and/or K14 are involved in cystine linkages in keratinocytes. Notably, all the cysteine residues in K5 or K14 are located in either the head or 2B domains. Additional studies are needed to understand the function of cysteines located in the head domains.

Several elements support the view that the homotypic, K14 Cys367–mediated *trans*-dimer disulfide bonds occurs between, rather than within, keratin filaments. First, the near-right angle between the two interacting coiled coils cannot be physically accommodated in the known architecture of 10-nm intermediate filaments[15], and there is limited rotational freedom about the cystine linkage. Second, the frequency of this bond is dramatically lower than the number of K5-K14 coiled-coil dimers in keratinocytes (**Fig. 3e**; ref. 36). Third, keratin-associated cystine linkages are concentrated to a specific region within the cell: the perinuclear space. Finally, the yield of the K14 Cys367–mediated disulfide bond increases coincidently with a major reorganization of keratin filaments, from being predominantly in the

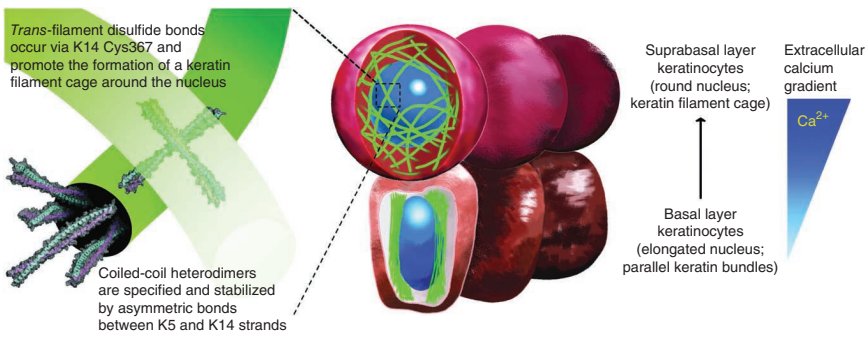

Figure 7 Model for the role of inter-filament cysteine linkages toward the organization and function of keratin filaments in the epidermis.

form of parallel bundles to crossing one another at a near-right angle, in cultured keratinocytes and in intact epidermis.

We propose a model in which the formation of homotypic, K14-mediated cystine linkages between keratin filaments fosters the formation of a specific intermediate filament network architecture in the perinuclear cytoplasm of epidermal keratinocytes (**Fig. 7**). We further posit, based on studies of keratinocytes in culture and of epidermis *in situ*, that the formation of these linkages is upregulated at an early stage of terminal differentiation, and that the resulting perinuclear cage of keratin filaments contributes to the resizing and reshaping of the nucleus in early differentiating keratinocytes (**Fig. 7**). Formation of such *trans*-filament disulfide bonds is a new mechanism to account for the organization of keratin filaments in epithelial cells. Our model asserts that these covalent linkages promote the formation of a stable and mechanically resilient network in which individual filaments cross one another at a particular angle. Cryo-EM studies performed on the uppermost cornified layers of epidermis have shown that keratin networks can either form parallel arrays or a cube-like structure[43]. In the 'cubic rod packing model' that resulted, keratin intermediate filaments are oriented at near-perpendicular angles, producing the highest strength-to-weight ratio and maximal network stiffness. Formation of interfilament disulfide bonds could have a role during the adoption of the cube-like architecture in corneocytes[43], a possibility supported by the presence of sulfhydryl oxidase in late-stage differentiating keratinocytes[44]. Moreover, K14 Cys367 is conserved in K10, a type I keratin expressed in copious amounts starting at an early stage of differentiation. Notably, K14 Cys367 does not occur in K15 or K19, two type I keratins enriched in skin epithelial stem cells[45].

The importance of the aberrations in the size and shape of nuclei in K14-null epidermis and the specific role of Cys367 in this finding are now revealed as open questions worth pursuing. Others[46] already showed that a keratinocyte precursor cell line derived from K14-null mice exhibits various anomalies in nuclear morphology and that induction of K17 expression as these cells mature in culture correlates with the loss of these aberrations (K14 Cys367 is conserved in K17). Vimentin was recently shown to help determine the position of the nucleus in an actin-dependent manner in migrating astrocytes in culture[47]. Additional issues of interest are the catalysis and regulation of the K14 Cys367–mediated cystine bond in keratinocytes. There are few examples of cytosolic proteins or oligopeptidyl compounds dimerizing via cystine linkages, for example, the Cu-Zn superoxide dismutase[48] and glutathione[49]. A clever study using a redox-sensitive YFP reporter showed that the cytosol, although strongly reducing, is nevertheless capable of maintaining cystine linkages[50]. In the epidermis, the enzyme sulfhydryl oxidase mediates disulfide bond formation during differentiation[44]. Here again, more studies are needed to define the mechanism involved in the formation of cystine bonds linking K14 molecules, and possibly other keratins, in keratinocytes of the skin and related epithelia.

METHODS

Methods and any associated references are available in the online version of the paper.

Accession codes. Coordinates and structure factors for the K5–K14 coil 2B heteromeric complex has been deposited in the Protein Data Bank with code 3TNU.

Note: Supplementary information is available in the online version of the paper.

ACKNOWLEDGMENTS

We thank members of the Coulombe and Leahy laboratories for guidance and support, M. Becker and N. Venugopalan for beamline assistance, and S. Bailey for comments. General Medicine and Cancer Institutes Collaborative Access Team receives support from the US National Cancer Institute (Y1-CO-1020) and the National Institute of General Medical Sciences (Y1-GM-1104). Use of the Advanced Photon Source was supported by the US Department of Energy, Basic Energy Sciences, Office of Science, under contract DE-AC02-06CH11357. These studies were otherwise supported by US National Institutes of Health grants AR42047 (to P.A.C.) and HD055545 (to D.J.L.).

AUTHOR CONTRIBUTIONS

C.-H.L. purified and crystallized the protein, analyzed the crystal structure, and performed *in silico*, *in vitro* and *in vivo* experiments. M.-S.K. collected, processed and refined the crystallographic data. B.M.C. performed the reconstitution experiment in A431 keratinocytes. D.J.L. aided in experimental design and provided guidance for several aspects of crystallography. P.A.C. designed the study, analyzed the data and wrote the manuscript in collaboration with C.-H.L., M.-S.K., B.M.C. and D.J.L.

COMPETING FINANCIAL INTERESTS

The authors declare no competing financial interests.

Published online at http://www.nature.com/doifinder/10.1038/nsmb.2330.
Reprints and permissions information is available online at http://www.nature.com/reprints/index.html.

1. Lazarides, E. Intermediate filaments as mechanical integrators of cellular space. *Nature* **283**, 249–256 (1980).
2. Fuchs, E. & Cleveland, D.W. A structural scaffolding of intermediate filaments in health and disease. *Science* **279**, 514–519 (1998).
3. Osborn, M. & Weber, K. Tumor diagnosis by intermediate filament typing: a novel tool for surgical pathology. *Lab. Invest.* **48**, 372–394 (1983).
4. Omary, M.B., Coulombe, P.A. & McLean, W.H.I. Intermediate filament proteins and their associated diseases. *N. Engl. J. Med.* **351**, 2087–2100 (2004).
5. Szeverenyi, I. *et al.* The Human Intermediate Filament Database: comprehensive information on a gene family involved in many human diseases. *Hum. Mutat.* **29**, 351–360 (2008).
6. Kim, S. & Coulombe, P.A. Intermediate filament scaffolds fulfill mechanical, organizational, and signaling functions in the cytoplasm. *Genes Dev.* **21**, 1581–1597 (2007).
7. Hanukoglu, I. & Fuchs, E. The cDNA sequence of a Type II cytoskeletal keratin reveals constant and variable structural domains among keratins. *Cell* **33**, 915–924 (1983).
8. Kim, S., Wong, P. & Coulombe, P.A. A keratin cytoskeletal protein regulates protein synthesis and epithelial cell growth. *Nature* **441**, 362–365 (2006).
9. Hatzfeld, M. & Weber, K. The coiled coil of in vitro assembled keratin filaments is a heterodimer of type I and II keratins: use of site-specific mutagenesis and recombinant protein expression. *J. Cell Biol.* **110**, 1199–1210 (1990).
10. Strelkov, S.V. *et al.* Conserved segments 1A and 2B of the intermediate filament dimer: their atomic structures and role in filament assembly. *EMBO J.* **21**, 1255–1266 (2002).
11. Steinert, P.M., Marekov, L.N., Fraser, R.D. & Parry, D.A. Keratin intermediate filament structure. Crosslinking studies yield quantitative information on molecular dimensions and mechanism of assembly. *J. Mol. Biol.* **230**, 436–452 (1993).
12. Bernot, K.M., Lee, C.H. & Coulombe, P.A. A small surface hydrophobic stripe in the coiled-coil domain of type I keratins mediates tetramer stability. *J. Cell Biol.* **168**, 965–974 (2005).
13. Franke, W.W. *et al.* Monoclonal cytokeratin antibody recognizing a heterotypic complex: immunological probing of conformational states of cytoskeletal proteins in filaments and in solution. *Exp. Cell Res.* **173**, 17–37 (1987).
14. Aebi, U., Haner, M., Troncoso, J., Eichner, R. & Engel, A. Unifying principles in intermediate filament assembly. *Protoplasma* **145**, 73–81 (1988).
15. Sokolova, A.V. *et al.* Monitoring intermediate filament assembly by small-angle x-ray scattering reveals the molecular architecture of assembly intermediates. *Proc. Natl. Acad. Sci. USA* **103**, 16206–16211 (2006).
16. Goldie, K.N. *et al.* Dissecting the 3-D structure of vimentin intermediate filaments by cryo-electron tomography. *J. Struct. Biol.* **158**, 378–385 (2007).
17. Strelkov, S.V. *et al.* Divide-and-conquer crystallographic approach towards an atomic structure of intermediate filaments. *J. Mol. Biol.* **306**, 773–781 (2001).
18. Strelkov, S.V., Schumacher, J., Burkhard, P., Aebi, U. & Herrmann, H. Crystal structure of the human lamin A coil 2B dimer: implications for the head-to-tail association of nuclear lamins. *J. Mol. Biol.* **343**, 1067–1080 (2004).
19. Krimm, I. *et al.* The Ig-like structure of the C-terminal domain of lamin A/C, mutated in muscular dystrophies, cardiomyopathy, and partial lipodystrophy. *Structure* **10**, 811–823 (2002).
20. Dhe-Paganon, S., Werner, E.D., Chi, Y.I. & Shoelson, S.E. Structure of the globular tail of nuclear lamin. *J. Biol. Chem.* **277**, 17381–17384 (2002).
21. Meier, M. *et al.* Vimentin coil 1A-A molecular switch involved in the initiation of filament elongation. *J. Mol. Biol.* **390**, 245–261 (2009).
22. Nicolet, S., Herrmann, H., Aebi, U. & Strelkov, S.V. Atomic structure of vimentin coil 2. *J. Struct. Biol.* **170**, 369–376 (2010).

23. Fuchs, E. Keratins and the skin. *Annu. Rev. Cell Dev. Biol.* **11**, 123–153 (1995).
24. Moll, R., Franke, W.W., Schiller, D.L., Geiger, B. & Krepler, R. The catalog of human cytokeratins: patterns of expression in normal epithelia, tumors and cultured cells. *Cell* **31**, 11–24 (1982).
25. Coulombe, P.A. & Fuchs, E. Elucidating the early stages of keratin filament assembly. *J. Cell Biol.* **111**, 153–169 (1990).
26. Lee, C.H. & Coulombe, P.A. Self-organization of keratin intermediate filaments into cross-linked networks. *J. Cell Biol.* **186**, 409–421 (2009).
27. Coulombe, P.A. *et al.* Point mutations in human keratin 14 genes of epidermolysis bullosa simplex patients: genetic and functional analyses. *Cell* **66**, 1301–1311 (1991).
28. Coulombe, P.A., Kerns, M.L. & Fuchs, E. Epidermolysis bullosa simplex: a paradigm for disorders of tissue fragility. *J. Clin. Invest.* **119**, 1784–1793 (2009).
29. Herrmann, H. & Aebi, U. Intermediate filaments: molecular structure, assembly mechanism, and integration into functionally distinct intracellular Scaffolds. *Annu. Rev. Biochem.* **73**, 749–789 (2004).
30. Parry, D.A., Fraser, R.D. & Squire, J.M. Fifty years of coiled-coils and alpha-helical bundles: a close relationship between sequence and structure. *J. Struct. Biol.* **163**, 258–269 (2008).
31. Vinson, C., Acharya, A. & Taparowsky, E.J. Deciphering B-ZIP transcription factor interactions in vitro and in vivo. *Biochim. Biophys. Acta* **1759**, 4–12 (2006).
32. Wu, K.C. *et al.* Coiled-coil trigger motifs in the 1B and 2B rod domain segments are required for the stability of keratin intermediate filaments. *Mol. Biol. Cell* **11**, 3539–3558 (2000).
33. Yasukawa, K., Sawamura, D., McMillan, J.R., Nakamura, H. & Shimizu, H. Dominant and recessive compound heterozygous mutations in epidermolysis bullosa simplex demonstrate the role of the stutter region in keratin intermediate filament assembly. *J. Biol. Chem.* **277**, 23670–23674 (2002).
34. Wilson, A.K., Coulombe, P.A. & Fuchs, E. The roles of K5 and K14 head, tail, and R/K L L E G E domains in keratin filament assembly in vitro. *J. Cell Biol.* **119**, 401–414 (1992).
35. Arslan, M., Qin, Z. & Buehler, M.J. Coiled-coil intermediate filament stutter instability and molecular unfolding. *Comput. Methods Biomech. Biomed. Engin.* **14**, 483–489 (2011).
36. Sun, T.T. & Green, H. Keratin filaments of cultured human epidermal cells. Formation of intermolecular disulfide bonds during terminal differentiation. *J. Biol. Chem.* **253**, 2053–2060 (1978).
37. Hennings, H. & Holbrook, K.A. Calcium regulation of cell-cell contact and differentiation of epidermal cells in culture. *Exp. Cell Res.* **143**, 127–142 (1983).
38. Feige, M.J. & Hendershot, L.M. Disulfide bonds in ER protein folding and homeostasis. *Curr. Opin. Cell Biol.* **23**, 167–175 (2011).
39. Chung, B.M., Murray, C.I., Van Eyk, J.E. & Coulombe, P.A. Identification of a novel interaction between Annexin A2 and Keratin 17: Evidence for reciprocal regulation. *J. Biol. Chem.* **287**, 7573–7581 (2012).
40. Crick, F.H. Is alpha-keratin a coiled coil? *Nature* **170**, 882–883 (1952).
41. O'Shea, E.K., Klemm, J.D., Kim, P.S. & Alber, T. X-ray structure of the GCN4 leucine zipper, a two-stranded, parallel coiled coil. *Science* **254**, 539–544 (1991).
42. Herrmann, H., Häner, M., Brettel, M., Ku, N.O. & Aebi, U. Characterization of distinct early assembly units of different intermediate filament proteins. *J. Mol. Biol.* **286**, 1403–1420 (1999).
43. Norlen, L. & Al-Amoudi, A. Stratum corneum keratin structure, function, and formation: the cubic rod-packing and membrane templating model. *J. Invest. Dermatol.* **123**, 715–732 (2004).
44. Hashimoto, Y. *et al.* Immunohistochemical localization of sulfhydryl oxidase correlates with disulfide crosslinking in the upper epidermis of rat skin. *Arch. Dermatol. Res.* **292**, 570–572 (2000).
45. Lyle, S. *et al.* The C8/144B monoclonal antibody recognizes cytokeratin 15 and defines the location of human hair follicle stem cells. *J. Cell Sci.* **111**, 3179–3188 (1998).
46. Troy, T.C. & Turksen, K. In vitro characteristics of early epidermal progenitors isolated from keratin 14 (K14)-deficient mice: insights into the role of keratin 17 in mouse keratinocytes. *J. Cell. Physiol.* **180**, 409–421 (1999).
47. Dupin, I., Sakamoto, Y. & Etienne-Manneville, S. Cytoplasmic intermediate filaments mediate actin-driven positioning of the nucleus. *J. Cell Sci.* **124**, 865–872 (2011).
48. Arnesano, F. *et al.* The unusually stable quaternary structure of human Cu,Zn-superoxide dismutase 1 is controlled by both metal occupancy and disulfide status. *J. Biol. Chem.* **279**, 47998–48003 (2004).
49. Meister, A. & Anderson, M.E. Glutathione. *Annu. Rev. Biochem.* **52**, 711–760 (1983).
50. Ostergaard, H., Tachibana, C. & Winther, J.R. Monitoring disulfide bond formation in the eukaryotic cytosol. *J. Cell Biol.* **166**, 337–345 (2004).

ONLINE METHODS

Expression and purification of K5–K14 2B heterocomplex. Sequence encoding the 2B domain of K5 was subcloned, untagged, in plasmid pRSET-2b containing an ampicillin-resistance gene, and sequence encoding the 2B domain of K14 was cloned with a His_6 tag and myc tag in pT7-HMT vector containing a kanamycin-resistance gene. The two plasmids were both transformed into the Rosetta (DE3) pLysS competent cells (Novagen), and dual transformants were selected on LB agar plates with ampicillin and kanamycin. Dual transformants were cultured in LB or M9 medium with both kanamycin and ampicillin, and protein production was induced with IPTG at 16 °C. To express a selenium-methionine–substituted K5–K14 2B complex, we used similar procedures except that once cultures reached OD_{600} ~0.7, the cultures were centrifuged, pelleted and resuspended in M9 medium containing selenomethionine and a high concentration of inhibitory amino acids for methionine synthesis (lysine, threonine, leucine, isoleucine, valine and phenylalanine) before adding IPTG. The soluble fraction of *Escherichia coli* cell lysates was subjected to a HiTrap Chelating HP column charged with nickel ion (GE Healthcare), which partitioned the K5–K14 coil 2B heteromeric complex and unbound K14 coil 2B protein into distinct fractions. Eluted fractions containing the heteromeric complex were next subjected to hydrophobic interaction chromatography (Phenyl HP, GE Healthcare) and Ni-NTA agarose (Qiagen) after removal of fusion tags with TEV protease. After removal of excess salt via dialysis, the K5–K14 heteromeric complex was purified using anion exchange chromatography (MonoQ, GE Healthcare), and concentrated using a centrifugal filter unit (Amicon Ultra, Millipore). All buffers used in the purification steps contained 10 mM β-mercaptoethanol.

Protein crystallization and data collection. Crystals of K5–K14 2B were grown at 20 °C via the hanging-drop vapor diffusion method by mixing 2 µl of K5–K14 2B protein solution (9 mg ml^{-1}) with an equal volume of reservoir solution containing 2.8 M NaCl and 0.1 M Tris-HCl (pH 8.5). Small crystals formed and were used to seed the same mixture of protein solution/reservoir solution, which yielded larger crystals. The resulting crystals belong to space group H32 and contain one K5–K14 heterodimer per asymmetric unit. A selenomethionine derivative of the K5-K14 2B complex gave rise to similar crystals under identical growth conditions. Before X-ray irradiation, crystals were transferred to a new reservoir solution containing 2.0 M NaCl and 0.1 M Tris-HCl (pH 8.5) in the sitting-drop plate and dehydrated overnight under a layer of paraffin oil. Dehydrated crystals were mounted frozen in liquid nitrogen stream before X-ray data collection. Selenium derivative data sets were collected at Advanced Photon Source beamline (Argonne National Laboratory) and processed with the software HKL2000 (ref. 51).

Structure determination and analyses. The structure was determined by SAD with SOLVE/RESOLVE[52] at 3.0 Å resolution. The model was built using COOT[53], refined using Phenix[54] and validated with the program Molprobity[55]. Selenium substitution identified nine of the ten methionine sites (five from K14 and four from K5; the N-terminal methionine of K5 is missing), adding confidence to the helix register assignment. Interactions between two monomers were assessed with LigPlot[56]. Homology modeling using the K5–K14 structure as a template was done using Modeller9.9 (ref. 57). Molecular images were generated using PyMol (The PyMol Molecular Graphics System, Version 1.2.0.1 Schrödinger, LLC). The electrostatic potential maps were calculated with APBS[58] via a PyMol plug-in and visualized with PyMol.

Site-directed mutagenesis to produce K14 variants. All constructs and point mutations were generated via a standard PCR-based cloning strategy using PfuUltra High Fidelity polymerase (Stratagene). Sequences encoding two distinct sets of K14 protein variants (K14-C367A, K14-C389A and wild-type K14), untagged and GFP-tagged at the N terminus, were built into a pBK-CMV mammalian vector backbone to characterize K14-dependent disulfide-bond formation in transfected keratinocytes.

Forced oxidation of K5 2B complexed with K14 2B or K5 2B complexed with K14 2B-tail. Dichloro(1,10-phenanthroline)-copper (Aldrich) was dissolved in DMSO to make a fresh stock solution and diluted to a final concentration of 300 mM for experiments. The stock solution was diluted to 1:60 (v/v) with the polypeptide solution of K5–K14 2B domains in 1× PBS buffer. The mixture was incubated for 30 min at room temperature, then quenched with 5 mM EDTA. To reverse the disulfide bond into free sulfhydryl groups, the quenched reaction solution was incubated with 5 mM TCEP for more than 1 h.

Analyses of keratins from skin tissue or cell lines. Skin samples were collected from P2 mouse pups and minced with a razor blade. Keratin proteins were isolated by incubating skin slices in radioimmune precipitation assay (RIPA) buffer (no reducing agent) containing 6 M urea. For cell experiments, mouse 308 keratinocyte cells were incubated with 1× TBS containing 1% Triton X-100, 1% NP-40 and 1 mM EDTA for 30 min to remove the plasma membrane and soluble proteins. After centrifugation-based sedimentation, the pelleted cytoskeletal fraction was collected. To assess formation of disulfide bonds, nonreducing SDS-PAGE followed by western blots were performed using a rabbit anti-GFP antibody (A11122; Invitrogen) or a rabbit polyclonal anti-K14 antibody (Covance), followed by a goat anti–rabbit antibody conjugated to horseradish peroxidase (Sigma-Aldrich). Enhanced chemiluminescence (Thermo Fisher Scientific) was performed according to the manufacturer's instructions. Imaging and quantification of the bands were performed using MutiImager III (Alpha Innotech).

Keratinocyte cell culture in high-calcium medium. Mouse 308 keratinocytes were grown in mKer medium[12]. For analyses involving the calcium-concentration switch[37], cultures were transferred to low-calcium medium (KBM-2, Lonza) on day 1, transferred to high-calcium medium (KBM-2 plus 1.8 mM $CaCl_2$) on day 2, and collected for analysis within 24 h.

Differential staining for disulfide bonds. The differential disulfide-bond staining method[59] was modified to localize cytoskeleton-bound cystine bonds by using extraction/fixation with organic solvents along with 1 mM Alexa Fluor 594 C_5-maleimide (Invitrogen). To stain for disulfide bonds in the cytoskeleton (insoluble compartment) of keratinocytes in culture *ex vivo* or in skin tissue *in situ*, samples were simultaneously extracted and chemically fixed with a prechilled 1:1 mixture of methanol and acetone at –20 °C for 5 min and washed with 1× PBS buffer at room temperature. To block the free sulfhydryl groups of cysteines not engaged in a disulfide bond, samples were incubated with 5 mM *N*-ethylmaleimide (NEM) in 1× PBS (pH 7.0) for 2 h at room temperature. Samples were washed with 1× TBS (pH 7.4) three times to quench the blocking reaction. To expose the sulfhydryl groups contained within disulfide bonds (oxidized state), the samples were incubated with 10 mM TCEP in 1× TBS (pH 7.4) for 1 h at room temperature. After washes in 1× PBS, samples were treated with 20 µM Alexa Fluor 594 C_5-maleimide in 1× PBS buffer (pH 7.0) for 2 h in the dark and at room temperature. Samples were then washed with prechilled 1× TBS to quench the reaction, and primary polyclonal antibody for K5 or K14 (Covance) at 1:1,000 dilution and Alexa Fluor 488–conjugated goat anti-rabbit secondary antibody (A11034; Invitrogen) at 1:1,000 dilution were sequentially applied at 4 °C in the dark.

Mouse lines. All experiments involving mice were reviewed and approved by the Institutional Animal Care and Use Committee. Mouse lines were maintained under specific pathogen-free conditions (SPF) and fed chow and water *ad libitum*. Keratin 14 hemizygous null mice[60] were maintained in a mixed-strain background. Genotyping was performed using PCR-based screening.

Immunostaining of skin tissue sections. P2 mouse pups were collected and decapitated; their dissected skin was flash-frozen in NEG50 mounting medium (Thermo Scientific), cryo-sectioned (8 µm thickness) and directly processed for staining. Immunostaining was done using a rabbit polyclonal antiserum to K14 (AF-64; Covance) at 1:1,000 dilution or a mouse monoclonal antiserum to K14 (LL001; Covance) at 1:1,000 dilution, and an Alexa Fluor 488–conjugated goat anti–rabbit or goat anti-mouse secondary antibody (Invitrogen) at 1:1,000 dilution. For immunostaining of K10, a rabbit polyclonal antibody (PRB-159P; Covance) at 1:1,000 dilution and PacificBlue-conjugated goat anti-rabbit secondary antibody (Invitrogen) at 1:500 dilution were used.

Rescue of type I keratin–deficient cells with K14 variants. Keratin 17 knockdown A431 cells[44] were grown in Dulbecco's modified Essential medium (Invitrogen) containing 10% FBS (Atlanta Biologicals), 100 units ml^{-1} penicillin, 100 µg ml^{-1} streptomycin (Invitrogen) and 0.5 µg ml^{-1} puromycin at 37 °C in 5% CO_2. Cells were transiently transfected with pBK-CMV His-GFP-K14

doi:10.1038/nsmb.2330

wild type, C367A or C389A using 4D-Nucleofector (Lonza), following the Amaxa Nucleofector 4D manual. We pulsed (Program DS-137) 375,000 trypsinized cells with 0.4 μg DNA in the nucleocuvette strip and plated the mixture on a cover slip (VWR) for analysis via immunofluorescence.

Microscopic imaging of cell and tissue preparations. Cell and tissue images were obtained at room temperature using a confocal microscope (Axiovert 200 microscope with a 510 Meta module; Carl Zeiss) fitted with a 40× 1.4 numerical aperture (NA) Plan-Apochromat oil objective and a 100× 1.4 NA Plan-Apochromat oil objective lenses. Microscope operation and image acquisition was done using the LSM 510 software (Carl Zeiss). For A431 cell images in **Figure 6**, a fluorescence microscope (AxioObserver inverted microscope with AxioCam MRm camera; Carl Zeiss) fitted with a 20× 0.8 NA Plan-Apochromat objective was used. Analysis of the dimensions of keratinocyte nuclei was performed using ImageJ software. Data were analyzed using the Microsoft Excel built-in *t*-test module.

51. Otwinowski, Z. & Minor, W. Processing of X-ray diffraction data collected in oscillation mode. in *Methods in Enzymology, Macromolecular Crystallography Part A* Vol. 276 (eds., Carter, C.W. Jr. & Sweet, R.M.) 307–326 (Academic Press, New York, 1997).
52. Terwilliger, T.C. SOLVE and RESOLVE: automated structure solution and density modification. *Methods Enzymol.* **374**, 22–37 (2003).
53. Emsley, P. & Cowtan, K. Coot: model-building tools for molecular graphics. *Acta Crystallogr. D Biol. Crystallogr.* **60**, 2126–2132 (2004).
54. Adams, P.D. *et al.* PHENIX: a comprehensive Python-based system for macromolecular structure solution. *Acta Crystallogr. D Biol. Crystallogr.* **66**, 213–221 (2010).
55. Davis, I.W. *et al.* MolProbity: all-atom contacts and structure validation for proteins and nucleic acids. *Nucleic Acids Res.* **35**, W375–W383 (2007).
56. Wallace, A.C., Laskowski, R.A. & Thornton, J.M. LIGPLOT: a program to generate schematic diagrams of protein-ligand interactions. *Protein Eng.* **8**, 127–134 (1995).
57. Eswar, N. *et al.* Comparative Protein Structure Modeling with MODELLER. in *Current Protocols in Bioinformatics* (suppl. 15) 5.6.1–5.6.30 (John Wiley & Sons, Inc., 2006).
58. Baker, N.A., Sept, D., Joseph, S., Holst, M.J. & McCammon, J.A. Electrostatics of nanosystems: application to microtubules and the ribosome. *Proc. Natl. Acad. Sci. USA* **98**, 10037–10041 (2001).
59. Pang, Y.Y., Schermer, A., Yu, J. & Sun, T.T. Suprabasal change and subsequent formation of disulfide-stabilized homo- and hetero-dimers of keratins during esophageal epithelial differentiation. *J. Cell Sci.* **104**, 727–740 (1993).
60. Lloyd, C. *et al.* The basal keratin network of stratified squamous epithelia: defining K15 function in the absence of K14. *J. Cell Biol.* **129**, 1329–1344 (1995).